INTERNATIONAL JOURNAL FOR NUMERICAL METHODS IN FLUIDS
Int. J. Numer. Meth. Fluids 2007; **53**:305–332
Published online 6 July 2006 in Wiley InterScience (www.interscience.wiley.com). DOI: 10.1002/fld.1281

Numerical simulation of flows around two circular cylinders by mesh-free least square-based finite difference methods

H. Ding[1], C. Shu[1,*,†], K. S. Yeo[1] and D. Xu[2]

[1]*Department of Mechanical Engineering, National University of Singapore, 10 Kent Ridge Crescent, Singapore 117576, Singapore*
[2]*Institute of High Performance Computing, 1 Science Park Road, #01-01 The Capricorn, Singapore 117528, Singapore*

SUMMARY

In this paper, the mesh-free least square-based finite difference (MLSFD) method is applied to numerically study the flow field around two circular cylinders arranged in side-by-side and tandem configurations. For each configuration, various geometrical arrangements are considered, in order to reveal the different flow regimes characterized by the gap between the two cylinders. In this work, the flow simulations are carried out in the low Reynolds number range, that is, $Re = 100$ and 200. Instantaneous vorticity contours and streamlines around the two cylinders are used as the visualization aids. Some flow parameters such as Strouhal number, drag and lift coefficients calculated from the solution are provided and quantitatively compared with those provided by other researchers. Copyright © 2006 John Wiley & Sons, Ltd.

Received 21 August 2003; Revised 19 November 2005; Accepted 20 April 2006

KEY WORDS: mesh-free; meshless; circular cylinder; Navier–Stokes equations; flow interference

1. INTRODUCTION

The studies of flow around one or arrays of circular cylinders are of practical importance in engineering. In many areas of engineering, circular cylinders form the basic component of structures, for example, heat exchange tubes, cooling systems for nuclear power plants, offshore structures, cooling towers, chimney stacks and transmission cables, etc. The engineering structures mentioned above are exposed to either air or water flow, and therefore they experience flow-induced vibration, which could lead to the structure failure under severe conditions. To avoid the situations mentioned above and improve the structure design, it is necessary for engineers to understand the details of the fluid–structure interaction, and possess the ability to predict the force and response of the

*Correspondence to: C. Shu, Department of Mechanical Engineering, National University of Singapore, 10 Kent Ridge Crescent, Singapore 117576, Singapore.
†E-mail: mpeshuc@nus.edu.sg

cylinder-like structures. Fortunately, the knowledge concerned can be enriched by the experimental and numerical simulations.

In the past decades the incompressible flow past one cylinder has been well studied. Now it is already considered as a classical case for validating new numerical scheme. It is known that the flow field around one cylinder demonstrates a broad class of patterns. Depending on the value of Reynolds numbers, it can be developed into either steady or unsteady one. From the viewpoint of geometrical configuration, flow around two cylinders can be considered as an extension of one isolated cylinder. However, the corresponding problem is much more complicated. That is because the dynamic interaction between the shed vortices, shear layers and Krmn vortex sheets appears in the wake of the cylinders. Consequently, the wake behaves quite differently from that of one isolated circular cylinder. Due to the abundance of interesting flow features, flow past a pair of circular cylinders has attracted many research attentions.

The geometrical configurations of two circular cylinders, in general, can be categorized into side-by-side, tandem, and staggered arrangements with respect to the direction of the free stream flow. These configurations have been studied experimentally and numerically by some researchers in the past. Among the experimental studies, Bearman and Wadcock [1] used flow-visualization methods to investigate the evolution of flow interference behind two side-by-side circular cylinders, and provided some physical analysis and explanations of their experimental results. The wake evolution behind two side-by-side cylinders was also experimentally studied by Williamson [2]. His studies focused on the flows in the low Reynolds number range (50–200). He observed that for a certain range of the gap, the wake behind the side-by-side cylinders showed synchronized behaviour, i.e. anti-phase or in-phase. The early experimental studies of flow around two circular cylinders were reviewed by Zdravkovich [3], especially in the high Reynolds number range (10^3–10^5). He classified a variety of the flow regimes by the geometrical arrangements of cylinders. With the advent and rapid development of computer technology, the flow around two circular cylinders is also investigated numerically [4–8]. Stansby and Slaouti [4] studied the flow around two circular cylinders in side-by-side arrangement within the high Reynolds number range using an inviscid discrete-vortex method. His numerical results grossly reproduce the flow features found in experiments. The flows around two side-by-side circular cylinders at $Re = 100$ were studied by Chang and Song [6] using a mixed finite element/finite difference method. Their computation confirmed the existence of symmetric and asymmetric wake patterns observed in previous experiments. Slaouti and Stansby [5] used a random vortex method to model two-dimensional laminar flows around two circular cylinders at $Re = 200$ in tandem and side-by-side arrangements. They showed that laminar flow computation can be of some help on the prediction of large-scale structures of flow at high Reynolds numbers. Mittal *et al.* [7] employed a stabilized finite element scheme to study the flow around two circular cylinders at Reynolds numbers of $Re = 100$ and 1000 in tandem and staggered arrangements. Their study mainly focused on the variation of force coefficients of the two cylinders, and found that the downstream cylinder experiences large unsteady force as compared with one isolated cylinder. More recently, Meneghini and Saltara [8] used finite element method to investigate the flow interference between two cylinders in tandem and side-by-side arrangements at Reynolds number of $Re = 200$. They provided the vorticity contours and the evolution history of lift and drag coefficients, and observed that in the tandem arrangement, the mean value of drag coefficient of the downstream cylinder changes from negative to positive when the gap between two cylinder centres is greater than three times of the cylinder diameter.

In the previous numerical studies of flow around two circular cylinders, most of the simulations employed mesh-based methods, such as finite difference, finite element, or random vortex. Although

DOI: 10.1002/fld

the discrete vortex method used by Stansby [4] does not require a mesh, however, its computation is based on a potential flow assumption. In other words, this method is only suitable for the flow simulation in the very high Reynolds number range. In general, mesh-based methods need to employ grid-generation techniques such as multi-block, coordinate transformation or patched coordinates, and build up data structure to store detailed elemental information comprising all node-based or element-based connectivity. As a consequence, the accuracy of numerical solution depends strongly on the mesh properties. On the other hand, the construction of body-fitting meshes and transformation of governing equations are usually tedious and problem dependent. To eliminate the mesh-related drawbacks, the so-called *meshless* or *mesh-free* methods have been developed in recent years, and serve as alternative numerical approaches for computational mechanics. The term *meshless* or *mesh-free* refers to the ability of the method to construct functional approximation or interpolation entirely from the information at a set of knots, without any pre-specified connectivity or relationships among the knots. The mesh-free least square-based finite difference (MLSFD) method proposed by Ding *et al*. [9] is among the group of mesh-free methods. The implementation of MLSFD method greatly reduces the human labour and computer time on the grid generation. Before the mesh-free method is efficiently applied in industry for complex problems, its robustness and effectiveness must be examined at first. The present study is such an attempt to address the issues on the flow around two cylinders by solving Navier–Stokes equations with MLSFD algorithm.

In this paper, we provide our numerical solutions for the flows past two cylinders in the side-by-side and tandem arrangements at Reynolds numbers of 100 and 200. For each arrangement, cylinders are placed apart with various gaps between two cylinder centres. It is already known that the wake interference behind two cylinders is highly influenced by the gap between the cylinders, and there exists a so-called critical gap, which is used to classify the flow patterns behind the cylinder into several categories. Based on the experimental observation, a range of flow regimes characterized by a critical gap has been found by Williamson [2] and by Zdravkovich [3]. Williamson found three flow patterns characterized for the side-by-side arrangement, i.e. $T<2.2D$, $2.2D<T<5D$, $T>5D$, where T represents the transverse gap between the two cylinders and D the diameter of the circular cylinder. Zdravkovich [3] reported that three flow regimes can be observed for the cylinders placed in tandem: $L<1.2-1.8D$, $1.2-1.8D<L<3.4-3.8D$ and $L>4D$, where L represents the longitudinal gap between the two cylinders. As suggested by Zdravkovich [3], the value of the critical gap depends on the Reynolds number and may vary within a certain range. In the present study, numerical simulations are performed for the cases with the transverse gaps of $1.5D$, $3D$, and $4D$ in the side-by-side arrangement and the longitudinal gaps of $2.5D$ and $5.5D$ in the tandem arrangement, respectively. Our objective is to confirm the earlier experimental findings on interactive vortex shedding and provide quantitative analysis of the flow field around two cylinders in the low Reynolds number range. In order to get better understanding of the wake interference around the two cylinders, the flow past one single cylinder is also simulated and the solution is taken as a reference to flow past two cylinders. In this work, the two-dimensional incompressible Navier–Stokes equations in the vorticity-stream function form are taken as the governing equations. The single-value pressure condition is implemented to determine the value of the stream function on the two cylinder walls. To describe the flow pattern quantitatively, mean values of lift and drag coefficients (C_D and C_L) and Strouhal (St) number are computed and compared with available data in the literature. To illustrate the detailed fluid structures near the wake region behind the two circular cylinders, numerical visualization are presented in the form of vorticity contours and streamlines.

DOI: 10.1002/fld

2. METHODOLOGY

In this section, a brief description of MLSFD method is provided firstly. Then, the governing equations and boundary conditions related with flow around two circular cylinders are presented. Finally, an efficient node generation is discussed.

2.1. MLSFD method and its derivative approximation

The MLSFD method employed in this study was inspired from the development of traditional finite difference method. Essentially, both methods were originated from the Taylor series expansion. MLSFD uses multi-dimensional Taylor series expansion to construct the approximation of the derivatives of unknown functions while FD employs the one-dimensional Taylor series expansion. For example, the functional value of a generic function ϕ at the supporting knot (as shown in Figure 1) can be approximated by the functional value and its derivatives at the reference knot by using the two-dimensional Taylor series expansion,

$$\begin{aligned}\phi_i = \phi_0 &+ \Delta x_i \left(\frac{\partial \phi}{\partial x}\right)_0 + \Delta y_i \left(\frac{\partial \phi}{\partial y}\right)_0 + \frac{1}{2}(\Delta x_i)^2 \left(\frac{\partial^2 \phi}{\partial x^2}\right)_0 + \frac{1}{2}(\Delta y_i)^2 \left(\frac{\partial^2 \phi}{\partial y^2}\right)_0 \\ &+ (\Delta x_i)(\Delta y_i) \left(\frac{\partial^2 \phi}{\partial x \partial y}\right)_0 + \frac{1}{6}(\Delta x_i)^3 \left(\frac{\partial^3 \phi}{\partial x^3}\right)_0 + \frac{1}{6}(\Delta y_i)^3 \left(\frac{\partial^3 \phi}{\partial y^3}\right)_0 \\ &+ \frac{1}{2}(\Delta x_i)^2(\Delta y_i) \left(\frac{\partial^3 \phi}{\partial x^2 \partial y}\right)_0 + \frac{1}{2}(\Delta x_i)(\Delta y_i)^2 \left(\frac{\partial^3 \phi}{\partial x \partial y^2}\right)_0 + \cdots \end{aligned} \tag{1}$$

where the subscript 0 indicates the corresponding values at the reference knot, and subscript i indicates the corresponding values at the ith supporting point. The relative position of the reference node and the ith supporting point is defined by Δx_i ($\equiv x_i - x_0$) and Δy_i ($\equiv y_i - y_0$), where (x_i, y_i) and (x_0, y_0) denote the Cartesian coordinates of the ith supporting point and the reference node, respectively.

If Equation (1) is truncated to the third-order derivatives, it will have 9 unknown derivatives. Among them, two are the first-order derivatives, three are the second-order derivatives, and four

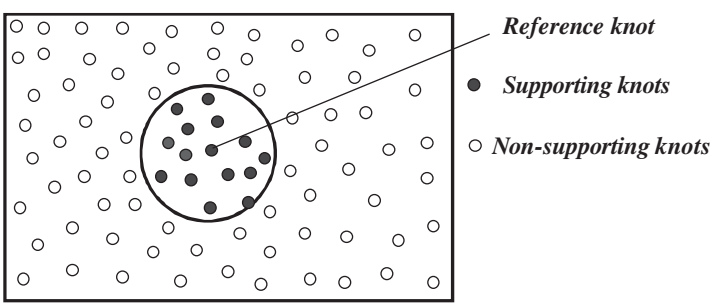

Figure 1. Supporting knots around a reference knot.

DOI: 10.1002/fld

are the third-order derivatives. To solve for the 9 unknowns, Equation (1) has to be applied at 9 neighbouring knots. As a result, the following matrix form is obtained:

$$\mathbf{\Delta\varphi} = \mathbf{S} \cdot \mathbf{d\varphi} \tag{2}$$

where

$$\mathbf{\Delta\varphi}^{\mathrm{T}} = [\phi_1 - \phi_0, \phi_2 - \phi_0, \ldots, \phi_9 - \phi_0]$$

$$\mathbf{d\varphi}^{\mathrm{T}} = \left[\left(\frac{\partial\phi}{\partial x}\right)_0 \quad \left(\frac{\partial\phi}{\partial y}\right)_0 \quad \left(\frac{\partial^2\phi}{\partial x^2}\right)_0 \quad \cdots \quad \left(\frac{\partial^3\phi}{\partial x\partial y^2}\right)_0 \right]$$

$$\mathbf{S} = \begin{pmatrix} \Delta x_1 & \Delta y_1 & \cdots & \frac{1}{2}\Delta x_1 \Delta y_1^2 \\ \Delta x_2 & \Delta y_2 & \cdots & \frac{1}{2}\Delta x_2 \Delta y_2^2 \\ \vdots & \vdots & & \vdots \\ \Delta x_9 & \Delta y_9 & \cdots & \frac{1}{2}\Delta x_9 \Delta y_9^2 \end{pmatrix}_{9\times 9}$$

and

$$\Delta x_i = x_i - x_0, \quad \Delta y_i = y_i - y_0, \quad i = 1, 2, \ldots, 9$$

Therefore, the derivative vector $\mathbf{d\varphi}^{\mathrm{T}}$ can be uniquely determined if the coefficient matrix $\mathbf{S}$ is not singular. However, for a set of randomly distributed nodes, the matrix $\mathbf{S}$ in Equation (2) does suffer the possible singularity. In the MLSFD method, the least-square technique is introduced to overcome this problem. The least-squares technique allows an optimized approximation derived from an over-determined set of equations, and the resultant matrix has good properties such as positive, symmetric, and definite. Thus, the problem of singular coefficient matrix is circumvented by means of using more supporting knots (more than the unknowns). More detailed descriptions about MLSFD method can be found in Reference [9].

The explicit expression for the optimal derivative approximation by the least-square technique can be written as

$$\mathbf{d\varphi} = (\mathbf{S}^{\mathbf{T}}\mathbf{S})^{-1}\mathbf{S}^{\mathbf{T}}\mathbf{\Delta\varphi} \tag{3}$$

Here, the row number of matrix $\mathbf{S}$ is usually larger than its column number. If they are of the same value and matrix $\mathbf{S}$ is invertible, the derivative vector derived from Equation (3) has the equivalent entries achieved by Equation (2). It should be noted that the use of least-square technique does not degrade the order of accuracy of finite-difference approximation [9]. Once the coefficient matrix is formed, it can be used to discretize the spatial derivatives in partial differential equations.

2.2. Governing equations

In the present study of flow around two circular cylinders, the flow is assumed to be viscous, laminar and incompressible. The governing equations are the two-dimensional, time-dependent

DOI: 10.1002/fld

Navier–Stokes equations and continuity equation written in the vorticity and stream function form. The non-dimensional governing equations can be expressed as

$$\frac{\partial \omega}{\partial t} + u\frac{\partial \omega}{\partial x} + v\frac{\partial \omega}{\partial y} = \frac{1}{Re}\left(\frac{\partial^2 \omega}{\partial x^2} + \frac{\partial^2 \omega}{\partial x^2}\right) \tag{4}$$

$$\frac{\partial^2 \psi}{\partial x^2} + \frac{\partial^2 \psi}{\partial y^2} = -\omega \tag{5}$$

where ψ denotes the stream function, ω represents the vorticity, and u, v denote the components of velocity in the x and y direction, which can be calculated from the stream function

$$u = \frac{\partial \psi}{\partial y}, \quad v = -\frac{\partial \psi}{\partial x} \tag{6}$$

An explicit scheme is developed to solve the above stream function-vorticity formulation. In the scheme, MLSFD method is responsible for the discretization of spatial derivatives and temporal discretization is based on an explicit Runge–Kutta method. With proper implementation of boundary conditions, the resultant algebraic equations are then solved in a time-marching manner.

2.3. Boundary and initial conditions

The geometry of flow domain and boundary conditions are depicted in Figure 2. The configuration of the two cylinders with equal diameter D, is defined by two parameters: the longitudinal gap L and transverse gap T. It is assumed that the two cylinders are immersed in steady free stream flow of velocity U, which is equivalent to impose the boundary condition for stream function with $\psi = U \cdot y$ and vorticity with $\omega = 0$. The top and bottom boundaries are located at a transversal distance of 12 times of the cylinder diameter, which is expected far enough to be the far-field. The out-flow boundary is extended to a distance of 25 times of the cylinder diameter downstream from the rear of the cylinder. The corresponding boundary condition is imposed in such a manner that

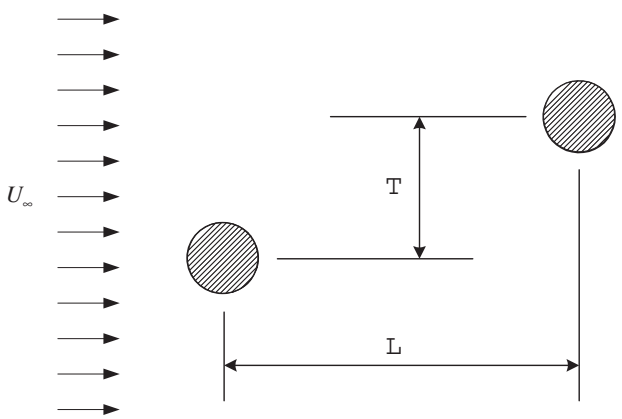

Figure 2. Geometrical description of flow past a pair of cylinders.

DOI: 10.1002/fld

it does not influence the vortices formed in the near wake of the cylinder. More precisely, we set

$$\frac{\partial \omega}{\partial x} = 0 \tag{7}$$

At the surface of the cylinder, the non-slip boundary condition applies, i.e. the velocity of the fluid is equal to the cylinder velocity, zero. Therefore, the stream function must satisfy two boundary conditions

$$\psi = \text{constant}, \quad \frac{\partial \psi}{\partial n} = 0 \tag{8}$$

There is no explicit boundary condition available for vorticity ω at the surface of cylinder, and it can be directly computed from the stream function.

2.3.1. Pressure single-value condition. In a multiply-connected domain, the value of the stream function at the surface of stationary body is a constant but unknown, which is determined and updated dynamically during the computation. To determine the value of the stream function on the wall, Tezduyar *et al*. [10] suggested using the single-value condition of the pressure for the multiply-connected domain. This condition is derived from the fact that the pressure is a scalar and can be formulated as

$$\oint_l \nabla p \, \mathrm{d}l = 0 \tag{9}$$

where l can be any line that makes an enclosure. In the present work, l is taken as the cylinder boundary along anti-clockwise direction. Therefore, Equation (9) can be simplified as

$$r \int_0^{2\pi} \frac{\partial p}{\partial \theta} \, \mathrm{d}\theta = 0 \tag{10}$$

The expression of $\partial p/\partial \theta$ on the cylinder wall can be derived from the momentum equation under the cylindrical coordinates, which is written as

$$\left.\frac{\partial p}{\partial \theta}\right|_{\text{inner}} = -R\frac{\partial^3 \psi}{\partial r^3} - \frac{\partial^2 \psi}{\partial r^2} \tag{11}$$

Substituting Equation (11) into Equation (10) gives

$$\int_0^{2\pi} \left(R\frac{\partial^3 \psi}{\partial r^3} + \frac{\partial^2 \psi}{\partial r^2} \right) \mathrm{d}\theta = 0 \tag{12}$$

The derivatives in Equation (12) can be discretized by the one-side finite difference schemes and expressed in terms of the stream function at the cylinder wall and interior knots. Substituting the derivative approximation forms into Equation (12), we can obtain the formulation of $\psi|_{\text{cylinder}}$. Then, the value of the stream function on the cylinder wall can be updated by the stream function values at the interior knots.

2.3.2. Initial condition. In this study, all the simulations are carried out in a time-marching manner. An unsymmetrical initial flow field, which serves as an artificial initiator for the numerical

DOI: 10.1002/fld

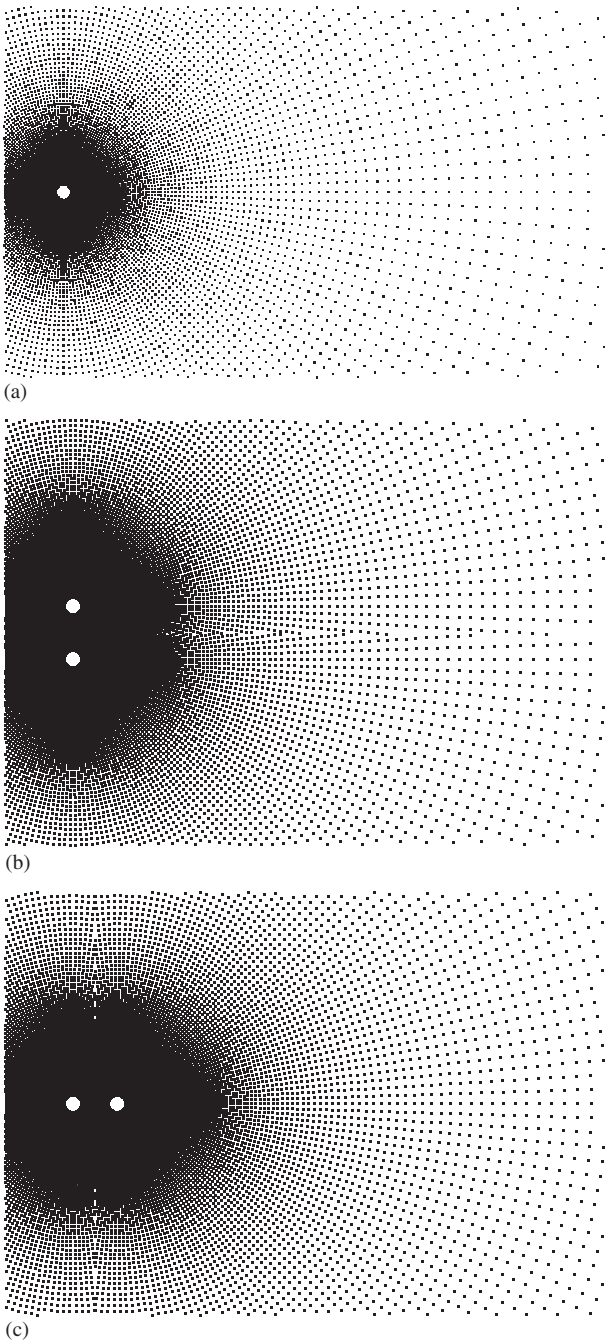

Figure 3. Three typical node distributions used in the present study: (a) one isolated cylinder; (b) side-by-side arrangement of $T = 3D$; and (c) tandem arrangement of $L = 2.5D$.

DOI: 10.1002/fld

simulation, is provided by

$$\psi = \sqrt{(x - x_c)^2 + (y - y_c)^2} \tag{13}$$

where x_c and y_c are the position of the centre of closest cylinder in the x and y coordinates, respectively. The initial values of vorticity in the domain are all set to zero. If the Reynolds numbers are less than some critical value, the introduced perturbation will be gradually dissipated by viscosity. If the Reynolds numbers are greater than the critical value, the introduced perturbation will trigger the vortex shedding process. For the cases of flow past two cylinders, the critical value of Reynolds numbers depends on the arrangements and the gaps of two cylinders.

2.4. Node generation

In principle, the concept of MLSFD discretization works well for any 'mesh' system, in which the nodes can be either regularly or irregularly distributed. This mesh-free property not only makes MLSFD method possess geometry flexibility, but also eases the procedure of node generation, especially for the cases in which geometrical complexity arise from the combination of multiple objects. For example, in the present study, though the computational domain is multiply-connected, the geometrical configuration is formed by several boundaries of simple shapes, i.e. circular cylinders and rectangular outer boundary. For each circular cylinder, the nodes in its neighbourhood can be generated by the use of the local cylindrical coordinate system. The only difference between the present node-generation technique and the one used for a single cylinder is that, in the middle of two cylinders, there is an invisible line, which forms the border of the two systems. The node-generation technique mentioned above is similar to the algorithm used in the overlapped mesh or the multi-block mesh generation. However, it removes their drawbacks such as information exchange between different meshes and mesh alignment near the region between different blocks. From the procedure of node generation described above, it is obvious that the mesh-free property of MLSFD method saves a lot of time and human labour in the 'grid' generation in the present two-cylinder cases as compared with traditional mesh-based methods. Following the procedures described above, three typical 'meshes' are generated for one isolated cylinder, two side-by-side cylinders and two tandem cylinders, respectively, which are shown in Figure 3. After the node generation, the local support of interior nodes must be determined before we do the mesh-free discretization. The neighbouring knots are found according to their distance to the reference node. For each reference node, we have to compute its distances to the surrounding knots first, and then list a sequence of neighbouring knots starting from the smallest one. When the number of neighbouring knots is given, it is easy to identify the neighbouring knots from the list. Some description about the selection of neighbouring knots was described in Reference [11].

3. RESULTS AND DISCUSSION

In this study, the MLSFD method is applied to simulate flows around two circular cylinders within the low Reynolds number range, i.e. $Re = 100$ and 200. Unless otherwise mentioned, the MLSFD scheme implemented for the spatial discretization is the second-order accurate for the second-order derivative approximation and the third-order accurate for the first-order derivative approximation. For each node inside the domain, 16 supporting points are employed to do the spatial discretization. To confirm the experimental observations, it is necessary to visualize the computational solution and provide the details of the flow near the wake region. Therefore, streamlines and vorticity

DOI: 10.1002/fld

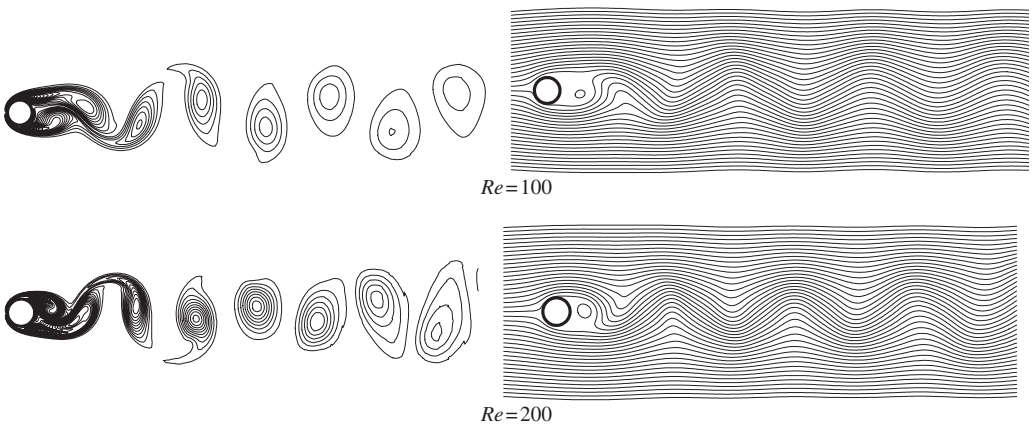

Figure 4. Instantaneous vorticity contours and streamlines of flow past one circular cylinder.

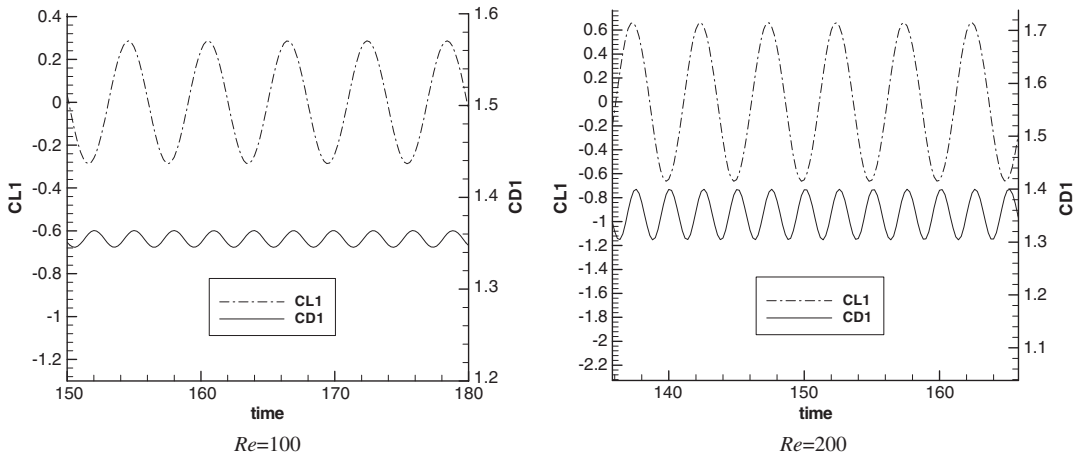

Figure 5. Drag and lift coefficients of flow past one cylinder.

Table I. Flow parameters for flow field around one circular cylinder at $Re = 100$ and 200.

Parameters	Drag coefficient (C_D)		Lift coefficient (C_L)		Strouhal number (St)	
Reynolds number	$Re = 100$	$Re = 200$	$Re = 100$	$Re = 200$	$Re = 100$	$Re = 200$
Belov *et al.* [12]	—	1.19 ± 0.042	—	± 0.64	—	0.193
Braza *et al.* [13]	1.364 ± 0.015	1.40 ± 0.05	± 0.25	± 0.75	0.160	0.200
Liu *et al.* [14]	1.350 ± 0.012	1.31 ± 0.049	± 0.339	± 0.69	0.164	0.192
Present	1.356 ± 0.010	1.348 ± 0.050	± 0.287	± 0.659	0.166	0.196

contours are plotted as the flow-visualization tools. Some flow parameters, which characterize the flow aspects such as lift and drag coefficients and Strouhal number, are also computed and quantitatively compared with the results of other researchers.

DOI: 10.1002/fld

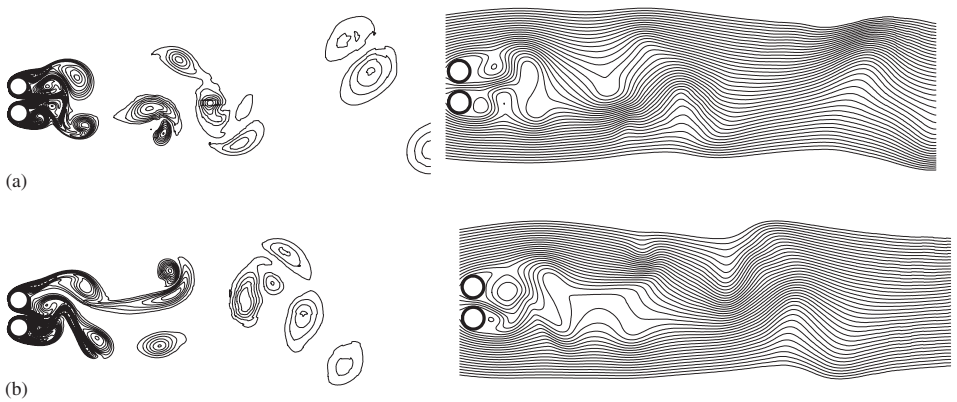

Figure 6. Instantaneous vorticity contours and streamlines for flow past a pair of side-by-side cylinders ($T = 1.5D$) at $Re = 200$: (a) non-dimensional time = 195; and (b) non-dimensional time = 201.

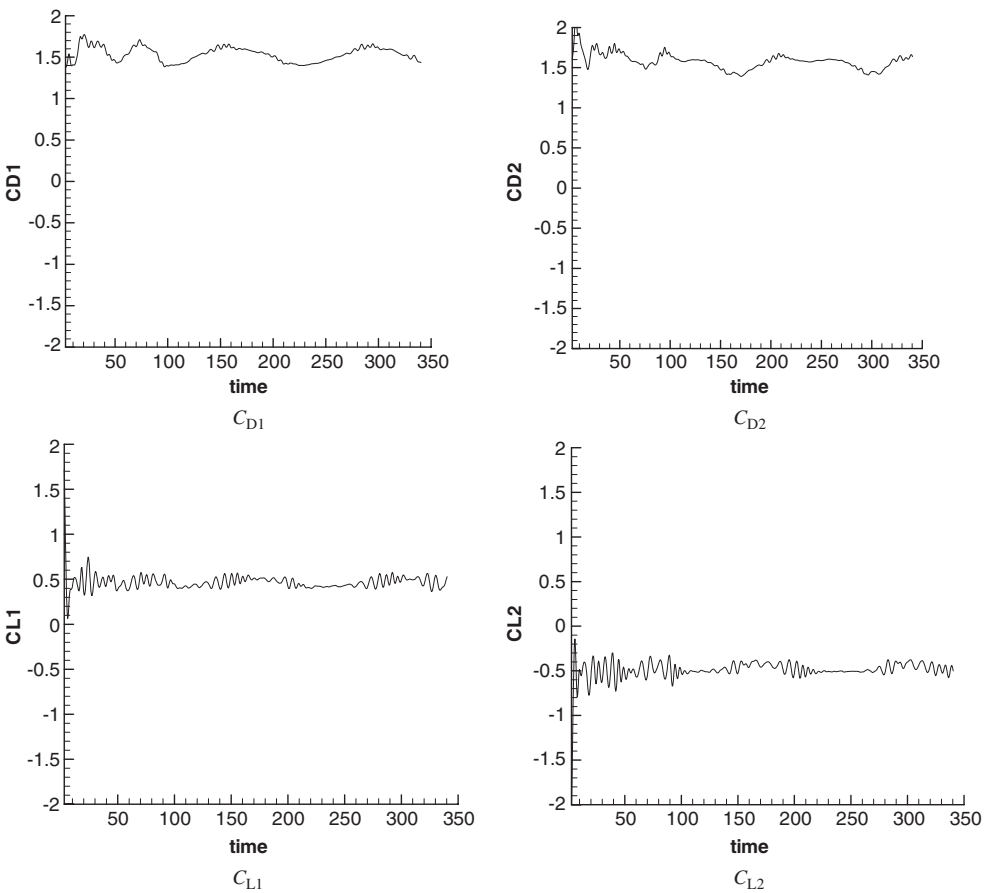

Figure 7. Time histories of drag (C_D) and lift (C_L) coefficients of flow past a pair of side-by-side cylinders ($T = 1.5D$) at $Re = 100$.

DOI: 10.1002/fld

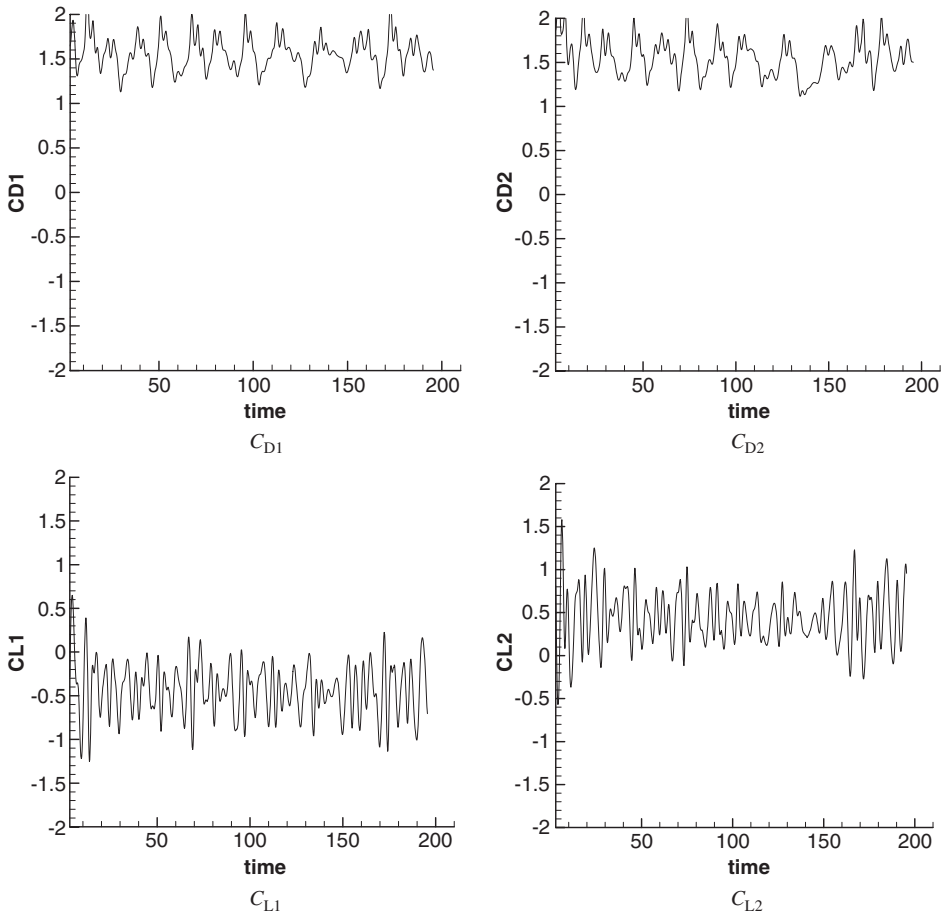

Figure 8. Time histories of drag (C_D) and lift (C_L) coefficients of flow past a pair of side-by-side cylinders ($T = 1.5D$) at $Re = 200$.

3.1. Definition of flow parameters

3.1.1. Lift and drag coefficients. In the viscous flow, the temporal histories of lift and drag forces are determined from the pressure distribution and friction at the surface of the blunt body. For the cases of flow around circular cylinders, the drag and lift can be obtained from

$$F_L = r \int \left(\mu r \frac{\partial \omega}{\partial n} - \mu \omega \right) \cos\theta \, d\theta$$
$$F_D = r \int \left(\mu r \frac{\partial \omega}{\partial n} - \mu \omega \right) \sin\theta \, d\theta \tag{14}$$

where r is the radius of the circular cylinder.

DOI: 10.1002/fld

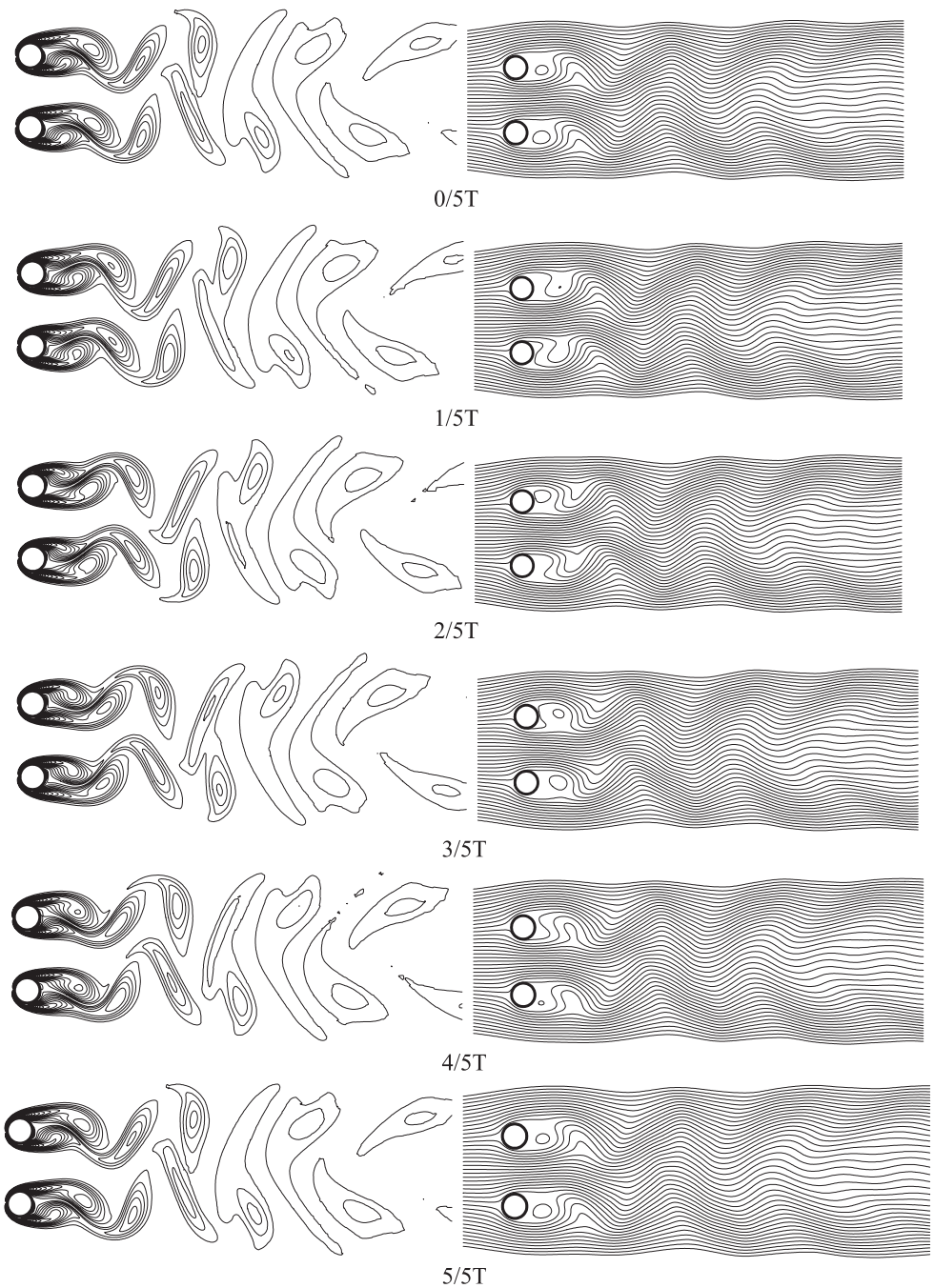

Figure 9. Instantaneous vorticity contours and streamlines for flow past a pair of side-by-side cylinders ($T = 3D$) at $Re = 100$ in a circle.

DOI: 10.1002/fld

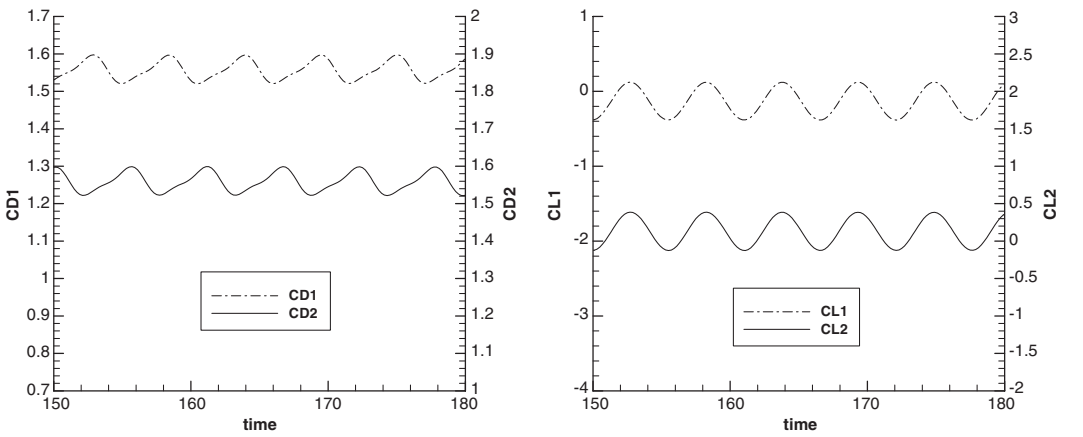

Figure 10. Drag and lift coefficients of flow past a pair of side-by-side cylinder ($T = 3D$) at $Re = 100$.

The non-dimensional drag and lift coefficients of the body are then given by

$$C_{\mathrm{L}} = \frac{2F_{\mathrm{L}}}{\rho U_{\infty}^2 D}, \quad C_{\mathrm{D}} = \frac{2F_{\mathrm{D}}}{\rho U_{\infty}^2 D} \tag{15}$$

3.1.2. Strouhal number. The Strouhal number (St) is used as a measure of the oscillating fluid flow phenomenon in the wake region. It is defined by the following relation:

$$St = f_{\mathrm{s}} \cdot D / U_{\infty} \tag{16}$$

where f_{s} is the shedding frequency and computed from the periodic evolution of the lift coefficient, D is cylinder diameter and U_{∞} is the velocity of free stream. Since D and U_{∞} are non-dimensionalized as unity, St is therefore equivalent to the shedding frequency.

3.2. Flow past an isolated circular cylinder

Flow past an isolated circular cylinder is a well-studied benchmark problem. One of its most attractive features is the vortex shedding behind the cylinder and the periodic variation of the flow field at moderate Reynolds number. To analyse and better understand the vortex shedding behaviour and the interference of vortex streets behind the two circular cylinders, the solution of flow past one cylinder can serve as a reference for comparison. Moreover, the study of flow past one cylinder can also be used to validate the present mesh-free scheme. In this study, the unsteady flow at $Re = 100$ and 200 are simulated on a 'mesh' with 23 033 nodes. The node distribution can be seen in Figure 3(a). As discussed in the previous section, the set of nodes are generated from a truncated polar mesh. The dimensionless time step is set to 0.005. At every time level, the convergence criterion of stream function-vorticity formulation is set in a manner that the residual is less than 10^{-6}. To obtain the characteristics of evolution of lift and drag coefficients, a long time of computation is necessary. In most of the cases, the computation runs for about 200 of dimensionless time, so does for the flow past two cylinders.

Figure 4 illustrates the typical vorticity contours and streamlines for $Re = 100$ and 200 at an instantaneous time. Figure 5 shows the time-dependent behaviour of the drag and lift coefficients

DOI: 10.1002/fld

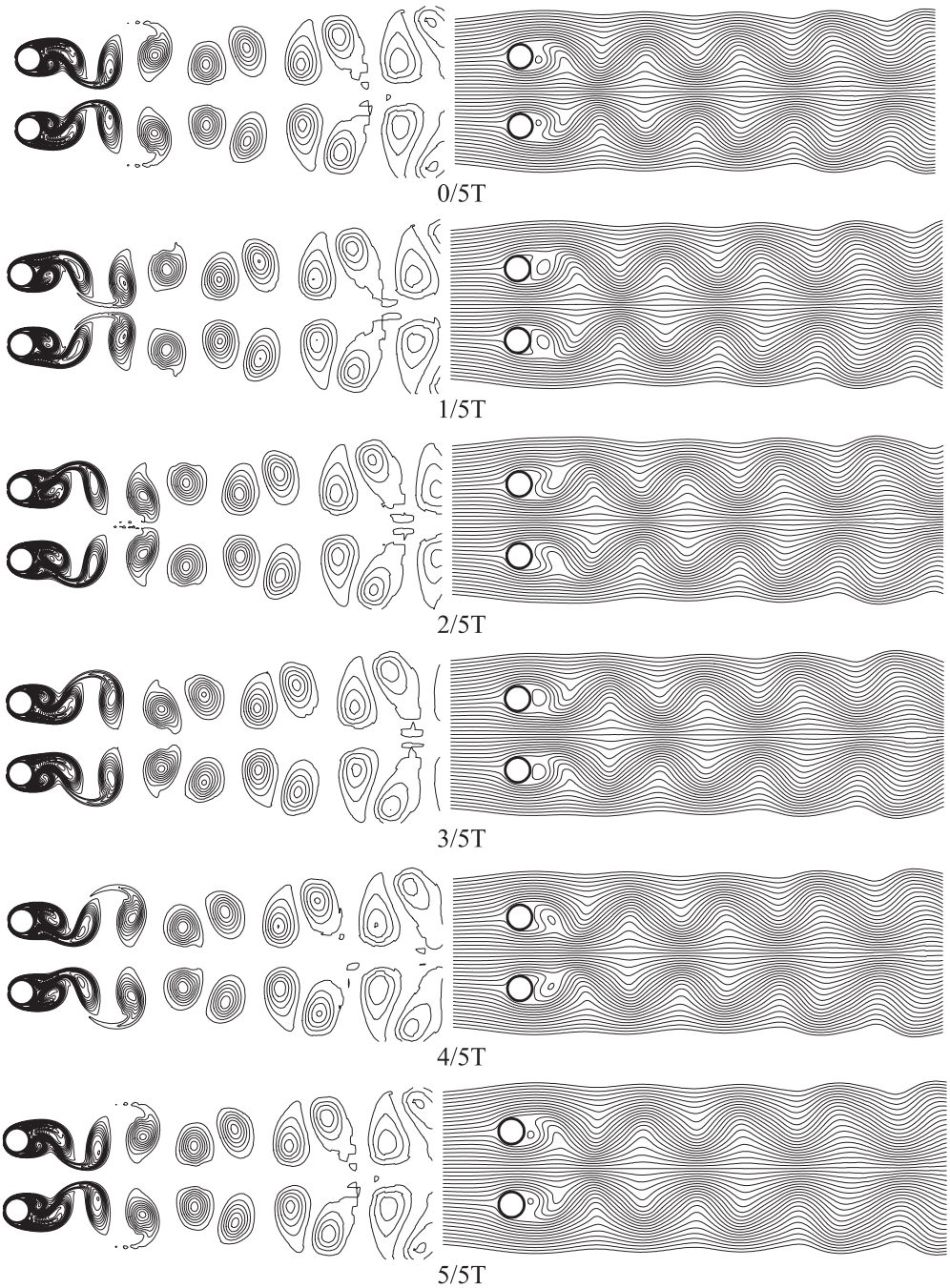

Figure 11. Instantaneous vorticity contours and streamlines for flow past two side-by-side cylinders ($T = 3D$) at $Re = 200$ in a circle.

DOI: 10.1002/fld

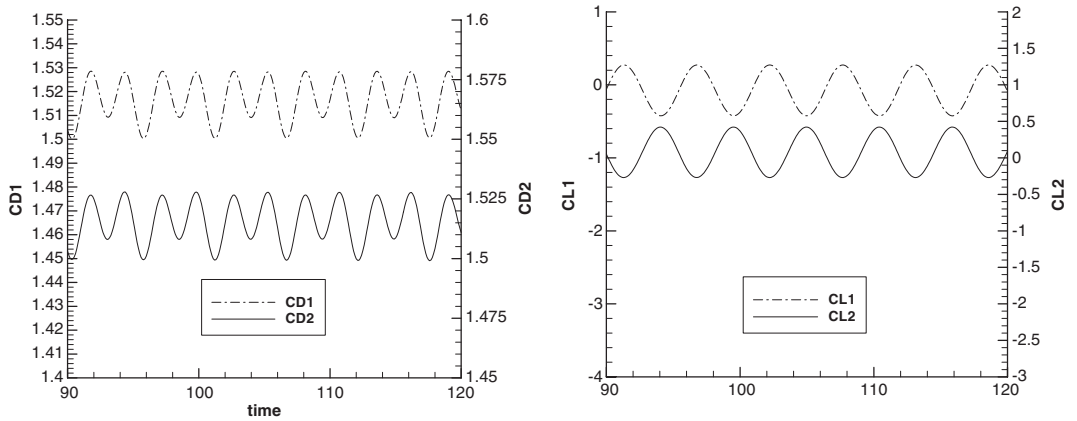

Figure 12. Drag and lift coefficients of flow past a pair of side-by-side cylinder ($T = 4D$) at $Re = 100$.

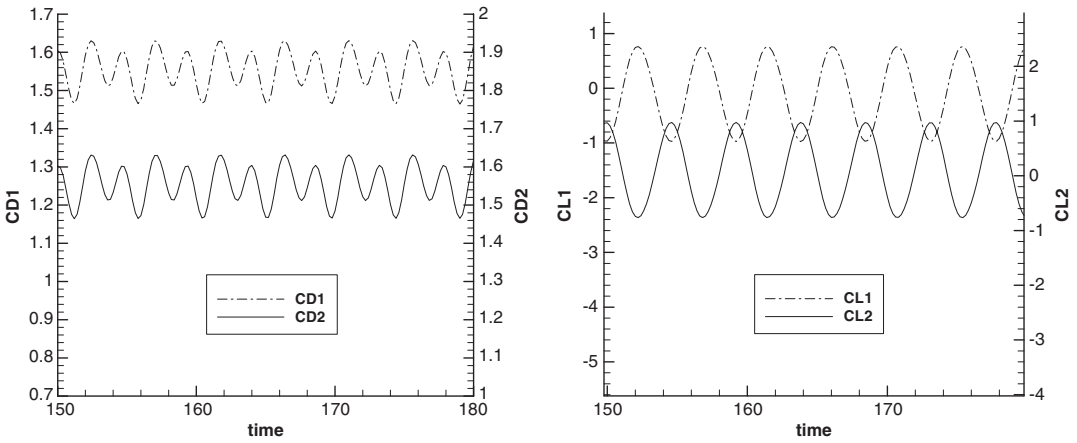

Figure 13. Drag and lift coefficients of flow past a pair of side-by-side cylinder ($T = 3D$) at $Re = 200$.

on the surface of cylinder for $Re = 100$ and 200. They both demonstrate clear periodicity, which implies the periodic vortex shedding from the rear surface of the cylinder. Table I lists the Strouhal number, mean value and amplitude of lift and drag coefficients of present results, as well as other published data from numerical investigations [12–14]. From Table I, it can be observed that our results agree very well with those achieved by other researchers. The mean values of drag coefficient of our solution differ from those of Liu *et al.* [14] by only about 0.4% at $Re = 100$, and 2.8% at $Re = 200$. The Strouhal number of present solution is 0.166 at $Re = 100$ and 0.196 at $Re = 200$. They are slightly greater than the results of Liu *et al.* [14], specifically about 1.2% at $Re = 100$ and 2.0% at $Re = 200$. The agreement on the flow parameters not only means that we obtain the reference results for the future analysis, but also indicates that the MLSFD method can be employed for the further study of flow around two circular cylinders.

DOI: 10.1002/fld

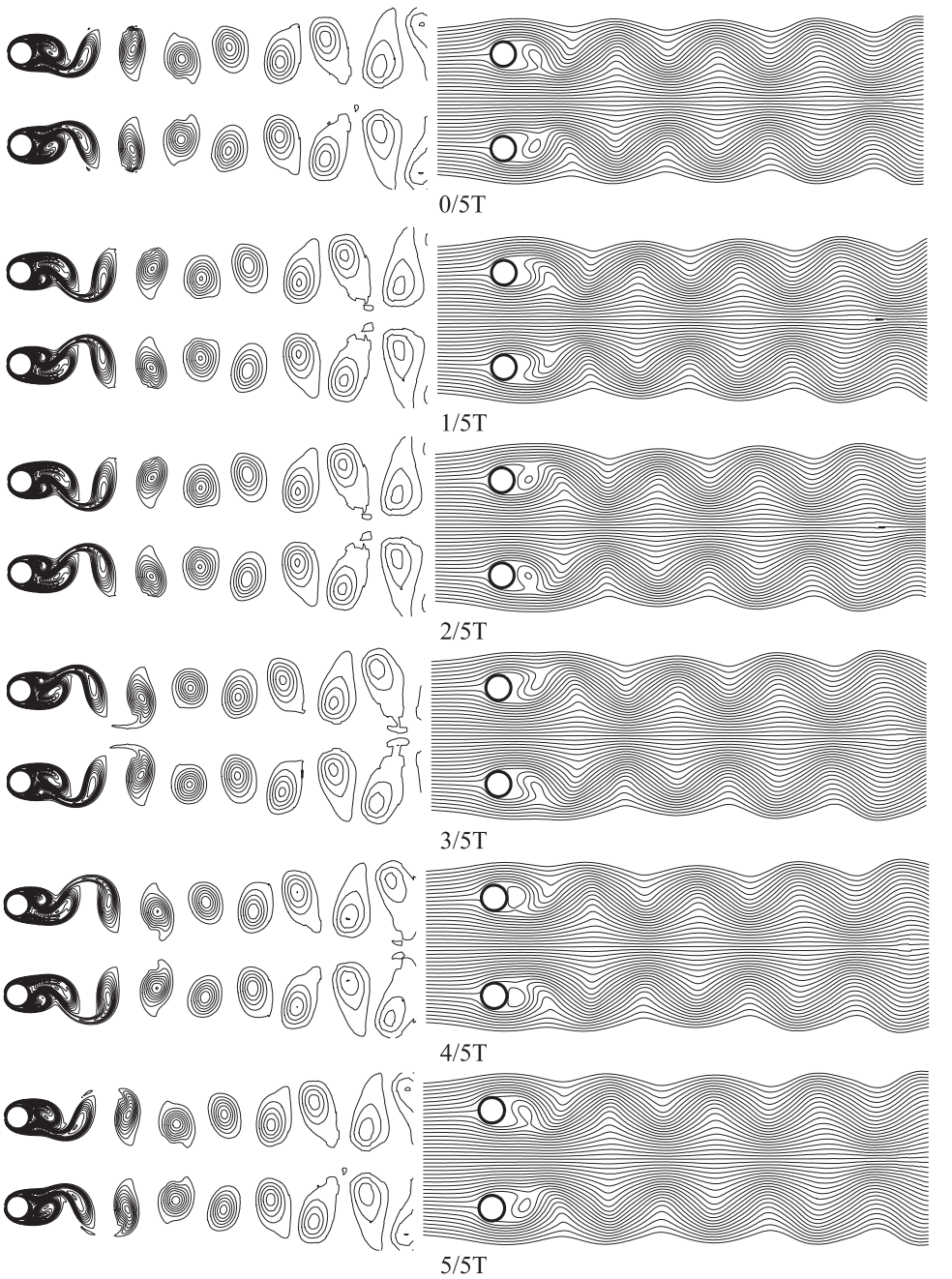

Figure 14. Instantaneous vorticity contours and streamlines for flow past a pair of side-by-side cylinders ($T = 4D$) at $Re = 200$ in a circle.

DOI: 10.1002/fld

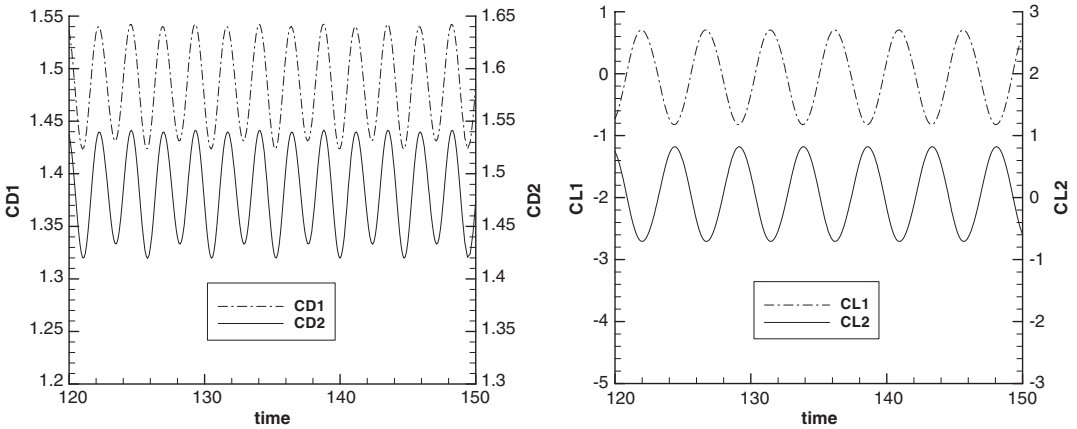

Figure 15. Drag and lift coefficients of flow past a pair of side-by-side cylinders ($T = 4D$) at $Re = 200$.

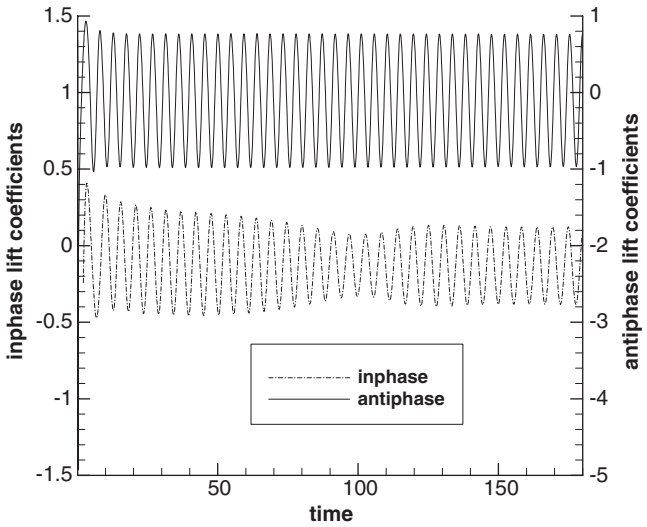

Figure 16. Time histories of in-phase and anti-phase lift coefficients for a pair of side-by-side cylinders ($T = 3D$).

3.3. Flow past two circular cylinders

As compared with the flow field behind one isolated circular cylinder, the flow fields behind two circular cylinders are much more complicated, especially for the case where the intense flow dynamic activity is noticed in the gap region between the cylinders. In this study, we mainly focused on the flow fields behind two cylinders arranged in side-by-side and tandem.

3.3.1. Side-by-side arrangement. In the side-by-side arrangement of two circular cylinders, numerical simulations have been performed for the cases of $T = 1.5D$, $3D$, and $4D$,

DOI: 10.1002/fld

Table II. Flow parameters for flow field around two circular cylinder at $Re = 100$ and 200.

Parameters		Drag coefficient (C_D)		Lift coefficient (C_L)		Strouhal number (St)	
Reynolds number		$Re = 100$	$Re = 200$	$Re = 100$	$Re = 200$	$Re = 100$	$Re = 200$
One isolated cylinder		1.356 ± 0.010	1.348 ± 0.050	0.00 ± 0.287	0.00 ± 0.659	0.166	0.196
$T = 1.5D$	Upper cylinder	1.53	1.54	−0.46	−0.41	—	—
	Lower cylinder	1.51	1.52	0.47	0.43	—	—
$T = 3D$	Upper cylinder	1.560 ± 0.038	1.548 ± 0.083	-0.131 ± 0.253	-0.104 ± 0.866	0.182	0.215
	Lower cylinder	1.560 ± 0.038	1.548 ± 0.083	0.131 ± 0.253	0.104 ± 0.866	0.182	0.215
$T = 4D$	Upper cylinder	1.514 ± 0.013	1.481 ± 0.0461	-0.077 ± 0.348	-0.058 ± 0.762	0.184	0.211
	Lower cylinder	1.514 ± 0.013	1.481 ± 0.0461	0.077 ± 0.348	0.058 ± 0.762	0.184	0.211

Table III. Comparison of flow parameters for side-by-side cylinders at $Re = 200$.

Parameters		Mean value of drag coefficient (C_D)		Mean value of lift coefficient (C_L)		Strouhal number (St)	
Results		Present	Meneghini [8]	Present	Meneghini [8]	Present	Meneghini [8]
$T = 1.5D$	Upper cylinder	1.54	1.32	−0.41	−0.40	—	—
	Lower cylinder	1.52	1.32	0.43	0.40	—	—
$T = 3D$	Upper cylinder	1.548	1.41	−0.104	−0.10	0.215	0.2
	Lower cylinder	1.548	1.41	0.104	0.10	0.215	0.2
$T = 4D$	Upper cylinder	1.481	1.34	−0.058	−0.05	0.211	0.2
	Lower cylinder	1.481	1.34	0.058	0.05	0.211	0.2

Table IV. Comparison of flow parameters for side-by-side cylinders at $Re = 100$.

Parameters		Drag coefficient (C_D)		Lift coefficient (C_L)		Strouhal number (St)	
Results		Present	Chang and Song [6]	Present	Chang and Song [6]	Present	Chang and Song [6]
$T = 3D$	Upper cylinder	1.560 ± 0.038	1.533 ± 0.04	-0.131 ± 0.253	-0.108 ± 0.31	0.182	0.18
	Lower cylinder	1.560 ± 0.038	1.533 ± 0.04	0.131 ± 0.253	0.108 ± 0.31	0.182	0.18

DOI: 10.1002/fld

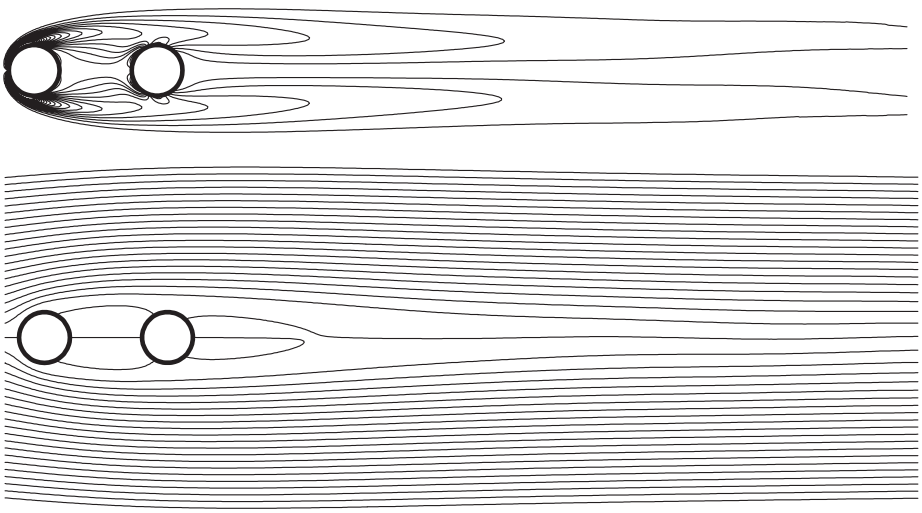

Figure 17. Instantaneous vorticity contours and streamlines for flow past a pair of tandem cylinders ($L = 2.5D$) at $Re = 100$.

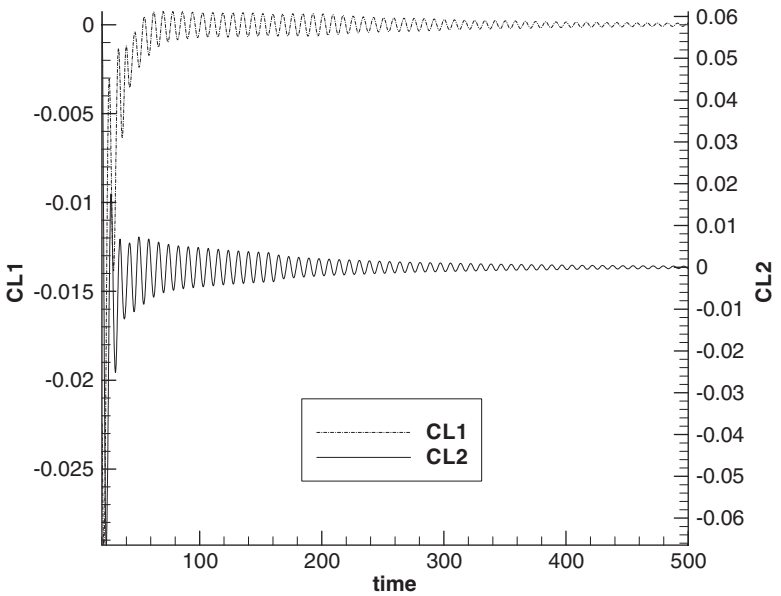

Figure 18. Time histories of lift (C_L) coefficients of flow past a pair of tandem cylinders ($L = 2.5D$) at $Re = 100$.

respectively. The node distributions are generated in the way as discussed in the previous section. A typical node distribution is depicted in Figure 3(b). The time step is set to the same value as in the one-cylinder case.

DOI: 10.1002/fld

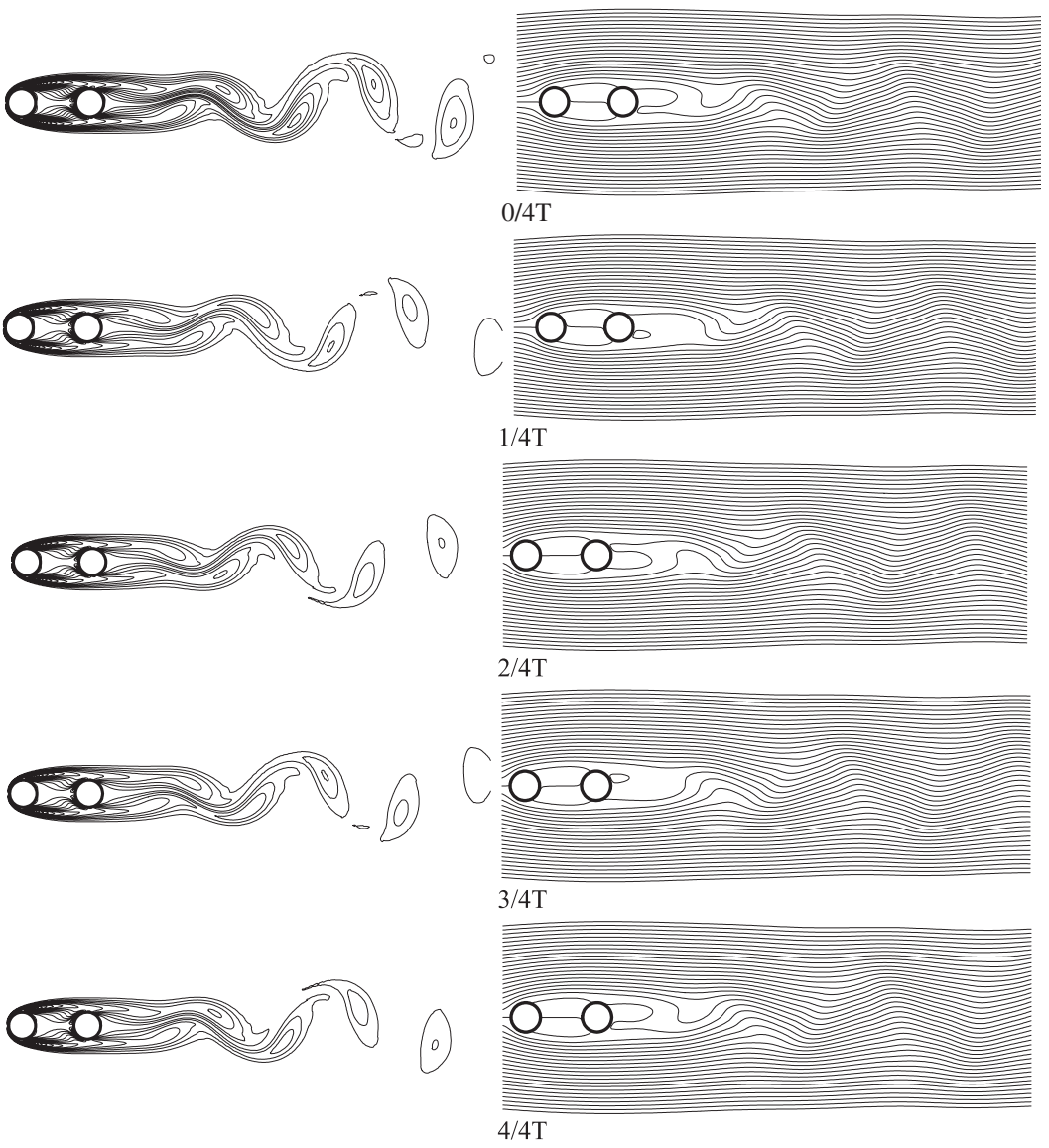

Figure 19. Instantaneous vorticity contours and streamlines for flow past a pair of tandem cylinders ($L = 2.5D$) at $Re = 200$ in a circle.

Figure 6 presents instantaneous vorticity contours and streamlines for the flow field of $T = 1.5D$ and $Re = 200$. The transverse gap of $1.5D$ is within the range of intermediate critical gap ($1.1D < T < 2.2D$) observed by Zdravkovich [3]. One of the characteristic features observed for this flow regime is the occurrence of biased flow pattern. Bearmann and Wadcock [1] and Williamson [2] observed in experiments that the biased flow pattern is bistable, i.e. the narrow and wide wakes, and the direction of the gap flow, switch from one cylinder to the other. This phenomenon is

DOI: 10.1002/fld

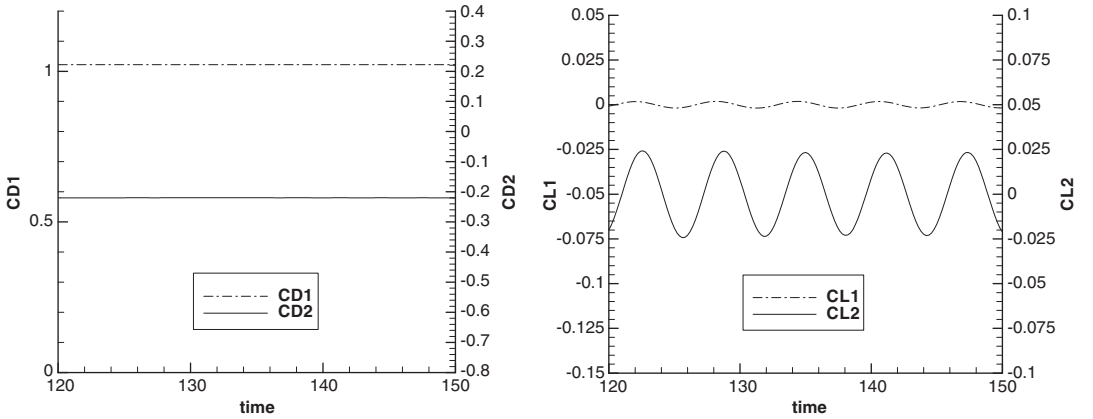

Figure 20. Drag and lift coefficients of flow past a pair of tandem cylinders ($L = 2.5D$) at $Re = 200$.

successfully reproduced as observed from the streamlines in Figure 6. Due to the similarity of flow pattern, the flow visualization is only provided for the flow at $Re = 200$. In Figures 7 and 8, the temporal histories of drag and lift coefficients are presented. From these figures, it can be observed that drag and lift coefficients exhibit irregular variation with time. It implies that the irregular vortex shedding occurs behind the pair of cylinders.

When the transverse gap is larger than $2D$, the occurrence of two synchronized Karman vortex streets are observed in the experiments for the side-by-side configuration [3]. Our numerical solutions for the flows of the transverse gap $T = 3D$ and $4D$ clearly reproduce this phenomenon as we observe the Figures 9, 11 and 14 in which the plots of instantaneous vorticity contours and streamlines are presented. The time evolutions of drag and lift coefficients are shown in Figures 10, 12, 13 and 15. As shown in these figures, the drag and lift coefficients synchronize variation with time, which also confirm the synchronized behaviour of vortex shedding from the upper and lower cylinders.

In the previous observation in experiments [1], two types of synchronized Karman vortex streets have been reported: symmetric (anti-phase) and anti-symmetric (in-phase). Both phenomena are also observed in our numerical experiments. In most cases, the flow behind two cylinders usually maintains anti-phase type of vortex streets. The only exception is the case of the transverse gap $T = 3D$ at $Re = 100$. In Figure 9, the instantaneous streamlines and vorticity contours within one cycle are provided. On the same 'mesh' and with the same initial condition, the flow of the transverse gap $T = 3D$ at $Re = 200$ finally reaches an anti-phase type of vortex shedding instead. The time histories of lift coefficients for the in-phase and anti-phase vortex shedding are shown in Figure 16. From the present numerical experiments, it is difficult to predict which type of flow pattern will occur or determine which type is more stable. Similar phenomenon has also been reported by Chang and Song [6]. However, from the comparison of time histories of lift coefficients shown in Figure 16, we can say that in-phase type of flow takes a much longer time to evolve into the final flow regime from the initial status as compared with its anti-phase counterpart.

Table II lists the Strouhal number, mean value and amplitude of lift and drag coefficients of present results at $Re = 100$ and 200. It can be observed that the mean value of lift coefficient is positive for the upper cylinder and negative for the lower cylinder. The reason may lie on the gap between the two cylinders, which prevents the flow going through. Therefore, a high-pressure

DOI: 10.1002/fld

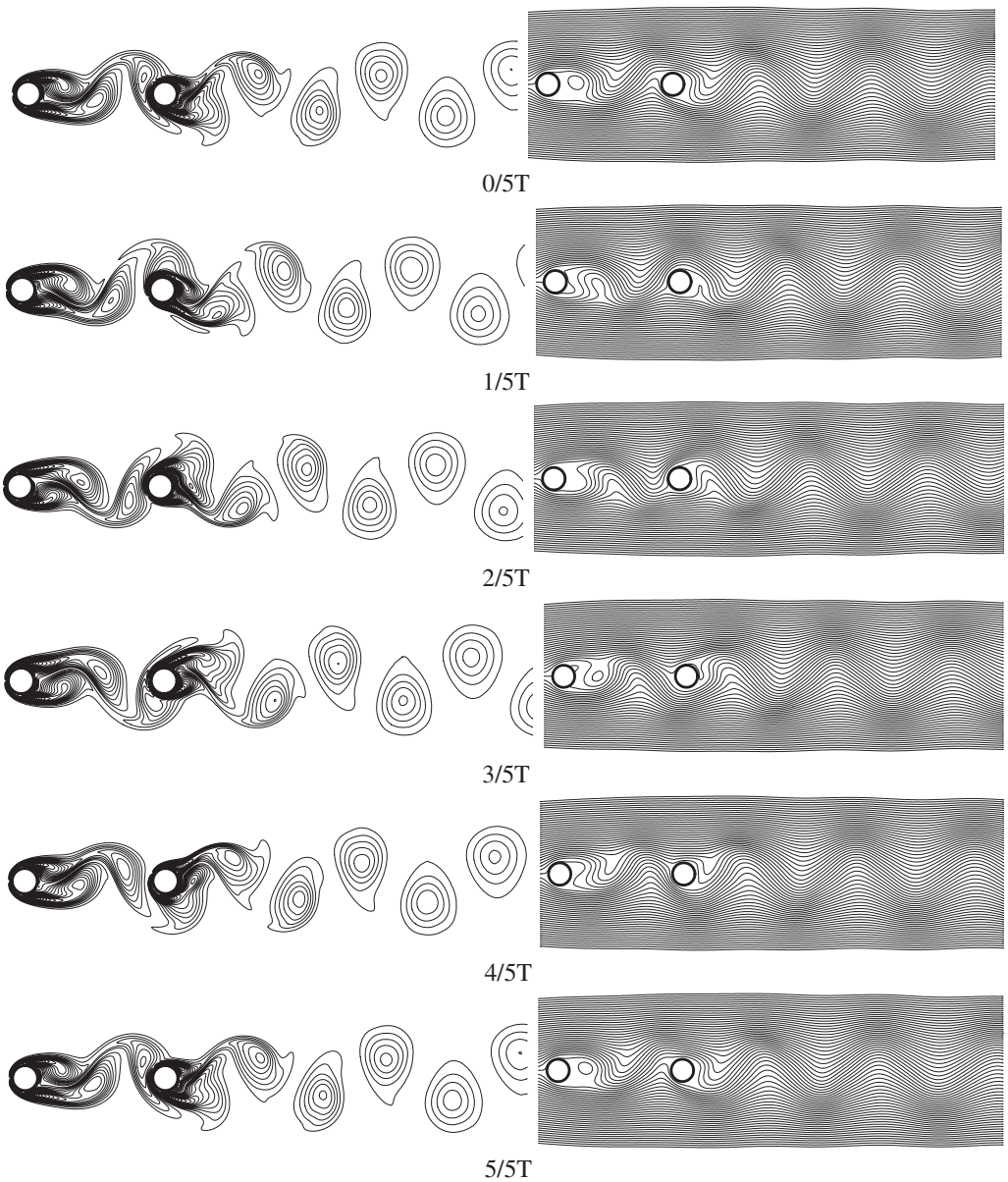

Figure 21. Instantaneous vorticity contours and streamlines for flow past a pair of tandem cylinders ($L = 5.5D$) at $Re = 100$ in a circle.

field is formed in the area between two cylinders. From Table II, it can also be observed that the flow parameters get closer to the solution of flow past one isolated cylinder as gap increasing. It indicates that less flow interference will be expected as the two cylinders are further apart.

DOI: 10.1002/fld

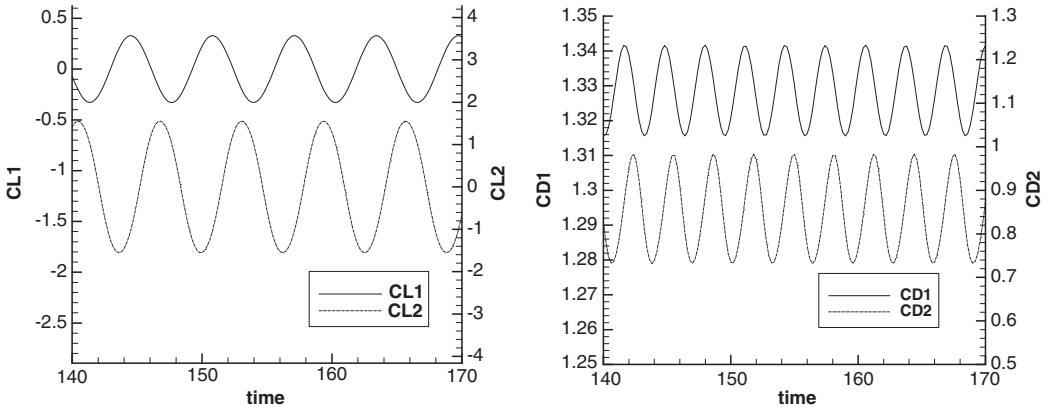

Figure 22. Drag and lift coefficients of flow past a pair of tandem cylinders ($P = 5.5D$) at $Re = 100$.

Table III presents our solutions and those of Meneghini and Saltara [8] at $Re = 200$. Table IV gives the comparison between our results and those of Chang and Song [6] at $Re = 100$. From the comparison, it can be seen that our calculated Strouhal numbers and lift coefficients are in good agreement with previously published data.

3.3.2. Tandem arrangement. In this section, numerical results pertaining to the flow past two cylinders in tandem are presented. In the present investigation, the longitudinal gaps between the two cylinders are $L = 2.5D$ and $5.5D$, respectively. A typical node distribution is depicted in Figure 3(c), which is for the case of $L = 2.5D$. Like the side-by-side arrangement, the time step is set to 0.005.

The streamlines and vorticity contours for the configuration of $L = 2.5D$ at $Re = 100$ are illustrated in Figure 17. It can be observed that the flow maintains a steady state though the Reynolds number is greater than the critical value for one isolated cylinder ($Re \approx 49$). From the streamline plots in Figure 17, we can also see that the flow going through the gap is restricted. Furthermore, the shear layer is separated from the inside surface of the upstream cylinder, and reattaches onto the outer surface of the downstream cylinder. This flow regime has been classified by Zdravkovich [15] as the quasi-steady reattachment. The temporal behaviour of lift coefficients for tandem cylinders of $L = 2.5D$ at $Re = 100$ are presented in Figure 18. From Figure 18, it can be observed that the amplitude of lift coefficients gradually decays as time advances, which reveals how the unsteady behaviour initially stirred by the artificial perturbation is gradually dissipated by viscosity. The flow field in the form of streamlines and vorticity contours for a higher Reynolds number ($Re = 200$) is shown in Figure 19. It can be seen that as the Reynolds number increases, the flow field behind the upstream cylinder remains steady, i.e. quasi-steady attachment, but it is not the case for the flow behind the downstream cylinder. The flow behind the downstream cylinder becomes unsteady at $Re = 200$, and finally evolves into an oscillatory pattern with obvious periodicity. The instantaneous streamlines and vorticity contours within one complete cycle are shown in Figure 19. The corresponding drag and lift coefficients are shown in Figure 20. It can be seen that the drag coefficients of both upstream and downstream cylinders keep constant but the lift coefficients vary with time.

DOI: 10.1002/fld

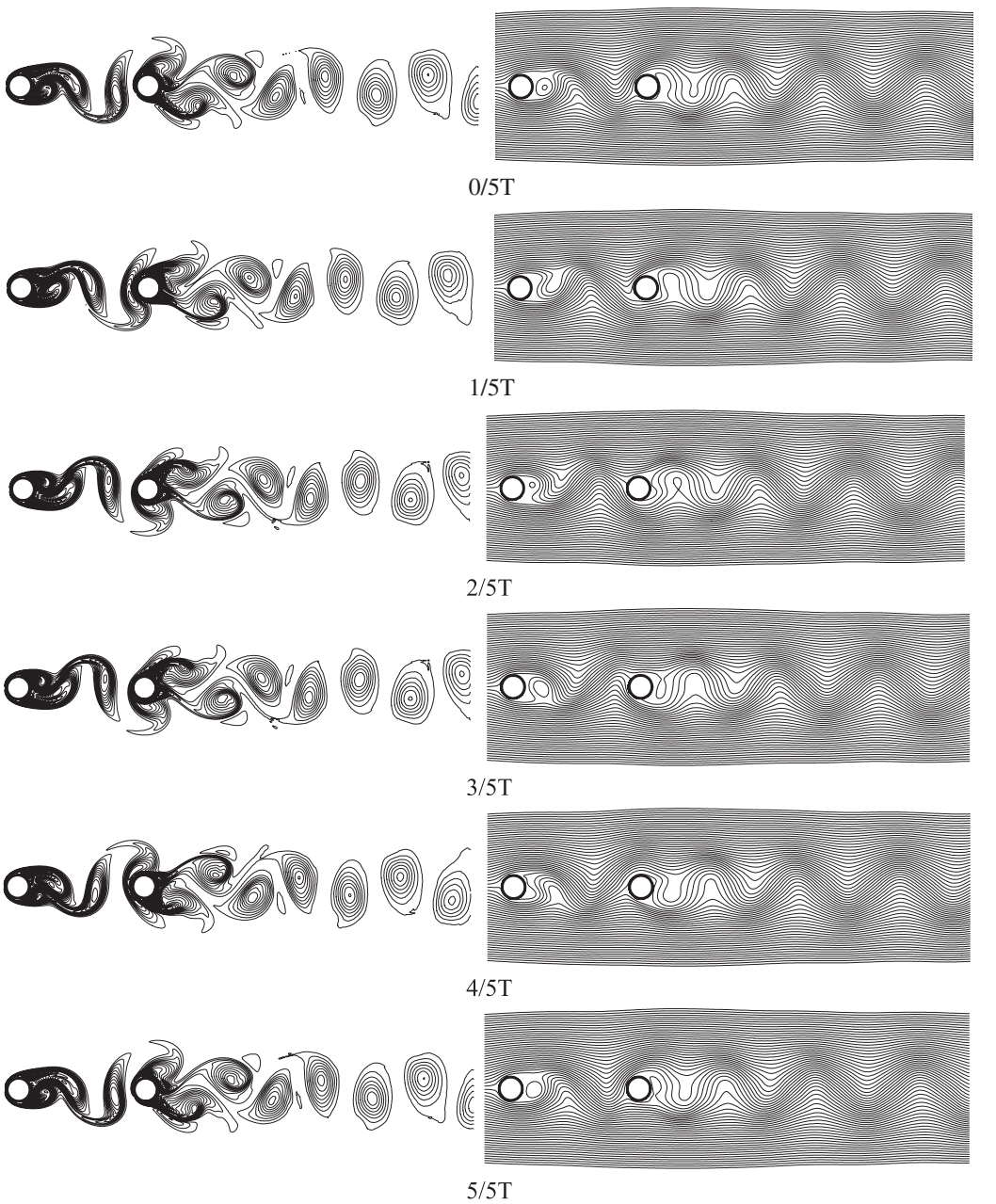

Figure 23. Instantaneous vorticity contours and streamlines for flow past a pair of tandem cylinders ($L = 5.5D$) at $Re = 100$ in a circle.

DOI: 10.1002/fld

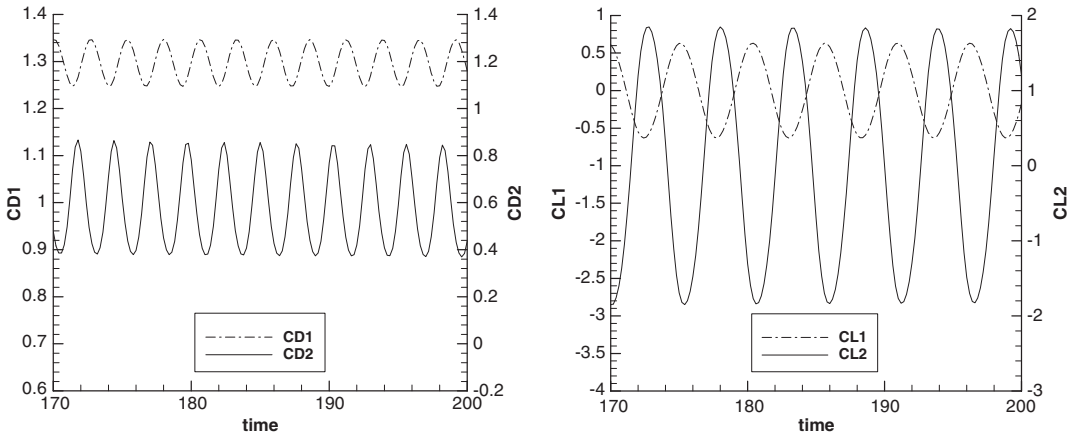

Figure 24. Drag and lift coefficients of flow past a pair of tandem cylinders ($L = 5.5D$) at $Re = 200$.

When the longitudinal gap between the two cylinders is increased from $2.5D$ to $5.5D$, the flow pattern in the gap region has a distinct change. In Figures 21 and 23, instantaneous streamlines and vorticity contours are shown for the flow fields at $Re = 100$ and 200 in one complete cycle. As observed from the streamline plots in Figures 21 and 23, the flow patterns are completely different from those for the cases of $L = 2.5$. The separated shear layer from the upstream cylinder no longer reattaches to the front of downstream cylinder. Instead, a Karman street is formed behind the upstream cylinder. From the vorticity contours, it is clear that vortex shedding from the downstream cylinder is highly disturbed by the impingement of the upstream vortex street. The temporal histories of drag and lift coefficients are shown in Figures 22 and 24. It can be seen that the lift coefficients of the upstream and downstream cylinders have the same frequency, and the synchronization occurs between the impingement flow and vortex shedding from the downstream cylinder. This 'lock-in' phenomenon is consistent to the findings of Rockwell [16] by experiments.

The *St* number, mean value and amplitude of drag and lift coefficients of our numerical results are listed in Table V. The results of flow past one isolated cylinder are also included in this table for comparison. It can be seen from Table V that when the gap between two cylinders is extended to $5.5D$, the flow parameters of upstream cylinder are very close to those of one isolated cylinder. But for the downstream cylinder, the solution difference with one isolated cylinder reflects the great influence of impingement flow on the flow field. Table VI presents the comparison of flow parameters between our solutions and those of Mittal *et al.* [7] at $Re = 100$. Overall, our results show good agreement with those of Mittal *et al.* [7].

3.3.3. Effects of Reynolds number. In the present studies, the numerical simulation is mainly carried out for the flow fields in the low Reynolds number range (i.e. $Re = 100$ and 200). The flow fields within high Re range (10^3–10^5) has not been performed due to lack of a good turbulence model. However, present numerical investigation shows some flow characteristics related with the Reynolds number, for example, Strouhal number. Similar to the flow past one circular cylinder, the Strouhal number tends to decreases as Reynolds number increases, which means the vortex shed from the cylinders at a faster speed. From the comparison of numerical solutions related

DOI: 10.1002/fld

Table V. Flow parameters for flow field around one circular cylinder at $Re = 100$ and 200.

Parameters		Drag coefficient (C_D)		Lift coefficient (C_L)		Strouhal number (St)	
Reynolds number		$Re = 100$	$Re = 200$	$Re = 100$	$Re = 200$	$Re = 100$	$Re = 200$
One isolated cylinder		1.356 ± 0.010	1.348 ± 0.050	0.00 ± 0.287	0.00 ± 0.659	0.166	0.196
$L = 2.5D$	Upstream cylinder	1.163	1.022	0.00	0.00 ± 0.0018	—	0.160
	Downstream cylinder	−0.0895	−0.220	0.00	0.00 ± 0.0233	—	0.160
$L = 5.5D$	Upstream cylinder	1.329 ± 0.013	1.295 ± 0.049	0.00 ± 0.330	0.00 ± 0.632	0.160	0.190
	Downstream cylinder	0.858 ± 0.125	0.608 ± 0.237	0.00 ± 1.554	0.00 ± 1.820	0.160	0.190

Table VI. Comparison of flow parameters for tandem cylinders at $Re = 100$.

Parameters		Drag coefficient (C_D)		Lift coefficient (C_L)		Strouhal number (St)	
Results		Present	Mittal *et al.* [7]	Present	Mittal *et al.* [7]	Present	Mittal *et al.* [7]
$L = 2.5D$	Upstream cylinder	1.163	1.271	0.0	0.0	—	—
	Downstream cylinder	−0.0895	−0.075	0.0	0.0	—	—
$L = 5.5D$	Upstream cylinder	1.329 ± 0.013	1.433 ± 0.015	0.0 ± 0.330	0.0 ± 0.403	0.160	0.168
	Downstream cylinder	0.858 ± 0.125	0.952 ± 0.164	0.0 ± 1.554	0.0 ± 1.741	0.160	0.168

with different Reynolds numbers, we observed that significant Reynolds number effects are mostly seen for the tandem configuration of two cylinders in terms of qualitative assessment of the flow regimes. The side-by-side configuration, on the other hand, is generally insensitive to Reynolds number. While the Reynolds number increases from 100 to 200, the flow regimes behind two cylinders remain the same for each geometrical configuration in the side-by-side arrangement, but show a distinct change in the tandem arrangement, especially for the geometrical configuration of $L = 2.5D$. The flow field behind the downstream cylinder develops from a steady state into an unsteady state as the Reynolds number increases.

4. CONCLUSIONS

In the present study, the flow fields around two circular cylinders arranged in tandem and side-by-side are numerically investigated by a mesh-free (MLSFD) method. The numerical simulations are carried out in the low Reynolds number range ($Re = 100$ and 200). The visualization of the numerical solutions is realized in terms of instantaneous streamlines and vorticity contours. It shows that the computational solutions reproduce the various flow regimes observed experimentally. Some

DOI: 10.1002/fld

flow parameters such as the St number, mean value and amplitude of drag and lift coefficients, which quantitatively characterize the flow fields, are provided, and compared well with those of previous studies.

The successful simulation of the complex flow phenomenon around two circular cylinders demonstrates the robustness and flexibility of present MLSFD method. However, for the practical application, the computational efficiency of the scheme is also an important issue for consideration. Taking this into account, a hybrid scheme, which combines the flexibility of mesh-free method and the high computational efficiency of the traditional FD schemes, may have a better potential in some cases [17].

REFERENCES

1. Bearman PW, Wadcock AJ. The interaction between a pair of circular cylinders normal to a stream. *Journal of Fluid Mechanics* 1973; **61**:499–511.
2. Williamson CHK. Evolution of a single wake behind a pair of bluff bodies. *Journal of Fluid Mechanics* 1985; **159**:1–18.
3. Zdravkovich MM. Review of flow interference between two circular cylinders in various arrangements. *Journal of Fluids Engineering* (ASME) 1977; **99**:618–633.
4. Stansby PK, Slaouti A. A numerical study of vortex shedding from one and two cylinders. *Aeronautical Quarterly* 1981; **32**:48–71.
5. Slaouti A, Stansby PK. Flow around two circular cylinders by the random-vortex method. *Journal of Fluids and Structures* 1992; **6**:641–670.
6. Chang KS, Song CJ. Interactive vortex shedding from a pair of circular cylinders in a transverse arrangement. *International Journal for Numerical Methods in Fluids* 1990; **11**:317–329.
7. Mittal S, Kumar V, Raghuvanshi A. Unsteady incompressible flows past two cylinders in tandem and staggered arrangements. *International Journal for Numerical Methods in Fluids* 1997; **25**:1315–1344.
8. Meneghini JR, Saltara F. Numerical simulation of flow interference between two circular cylinders in tandem and side-by-side arrangement. *Journal of Fluids and Structures* 2001; **15**:327–350.
9. Ding H, Shu C, Yeo KS. Development of least square-based two-dimensional finite difference schemes and their application to simulate natural convection in a cavity. *Computer and Fluids* 2004; **33**:137–154.
10. Tezduyar TE, Glowinski R, Liou J. Petrov–Galerkin methods on multiply connected domains for the vorticity-stream function formulation of the incompressible Navier–Stokes equations. *International Journal for Numerical Methods in Fluids* 1988; **8**:1269–1290.
11. Ding H, Shu C, Tang DB. Error estimates of local multiquadric-based differential quadrature (LMQDQ) method through numerical experiments. *International Journal for Numerical Methods in Engineering* 2005; **63**:1513–1529.
12. Belov A, Martinelli L, Jameson A. A new implicit algorithm with multigrid for unsteady incompressible flow calculation. *AIAA 95-0049*, January 1995; 9.
13. Braza M, Chassaing P, Ha Minh H. Numerical study and physical analysis of the pressure and velocity fields in the near wake of a circular cylinder. *Journal of Fluid Mechanics* 1986; **165**:79.
14. Liu C, Zheng X, Sung CH. Preconditioned multigrid methods for unsteady incompressible flows. *Journal of Computational Physics* 1998; **139**:35.
15. Zdravkovich MM. Flow induced oscillations of two interfering circular cylinders. *Journal of Sound and Vibration* 1985; **101**:511–521.
16. Rockwell D. Vortex-body interactions. *Annual Review of Fluid Mechanics* 1998; **30**:199–229.
17. Ding H, Shu C, Yeo KS, Xu D. Simulation of incompressible viscous flows past a circular cylinder by hybrid FD scheme and meshless least square-based finite difference method. *Computer Methods in Applied Mechanics and Engineering* 2004; **193**:727–744.

DOI: 10.1002/fld